EPJ manuscript No.
(will be inserted by the editor)

Ferromagnetic resonance study of sputtered Co|Ni multilayers

J-M. L. Beaujour[1], W. Chen[1], K. Krycka[3], C-C. Kao[3], J. Z. Sun[2] and A. D. Kent[1]

[1] Department of Physics, New York University - 4 Washington Place, New York, NY 10003, USA

[2] IBM T. J. Watson Research Center - Yorktown Heights, NY 10598, USA

[3] Brookhaven National Laboratory - Upton, New York 11973, USA

Received: date / Revised version: February 8$^{\text{th}}$ 2007

Abstract. We report on room temperature ferromagnetic resonance (FMR) studies of [t Co|2t Ni]×N sputtered films, where $0.1 \leq t \leq 0.6$ nm. Two series of films were investigated: films with same number of Co|Ni bilayer repeats (N=12), and samples in which the overall magnetic layer thickness is kept constant at 3.6 nm (N=1.2/t). The FMR measurements were conducted with a high frequency broadband coplanar waveguide up to 50 GHz using a flip-chip method. The resonance field and the full width at half maximum were measured as a function of frequency for the field in-plane and field normal to the plane, and as a function of angle to the plane for several frequencies. For both sets of films, we find evidence for the presence of first and second order anisotropy constants, K_1 and K_2. The anisotropy constants are strongly dependent on the thickness t, and to a lesser extent on the total thickness of the magnetic multilayer. The Landé g-factor increases with decreasing t and is practically independent of the multilayer thickness. The magnetic damping parameter α, estimated from the linear dependence of the linewidth, $\triangle H$, on frequency, in the field in-plane geometry, increases with decreasing t. This behaviour is attributed to an enhancement of spin-orbit interactions with t decreasing and in thinner films, to a spin-pumping contribution to the damping.

PACS. 72.47.-m Magnetotransport phenomena; materials for magnetotransport – 85.70.Kh Magnetic recording materials

1 Introduction

An understanding of magnetization dynamics in very thin ferromagnetic layers is central to the physics and application of spin-transfer, as devices are typically composed of layers only a few nanometers thick [1]. For example, the threshold current density for magnetic excitations is proportional to the magnetic damping parameter α, which can depend on the layer environment [2,3,4]. Further, in most spin-transfer devices, current-induced excitation involves precession of the magnetization out of the thin-film plane. The easy-plane anisotropy associated with the thin film geometry therefore plays a significant role in the resulting precession and reversal. It is also predicted to set the threshold current, since this anisotropy is often much larger than the in-plane anisotropy [5]. It is therefore of interest to vary the easy-plane anisotropy and experiment with layers with perpendicular magnetic anisotropy [5,6]. In fact, very recently Co|Ni multilayers were incorporated into spin-torque devices [7]. This magnetic multilayer system is interesting because it has a tunable easy-plane anisotropy, and devices which incorporate such layers exhibit a reasonable GMR. Early on, Daalderop *et al.* showed that evaporated Co|Ni multilayers exhibit large perpendicular magnetic anisotropy (PMA) and perpendicular magnetization [8]. In addition, it was shown that by varying the Co|Ni thickness ratio, it is possible to change the effective demagnetization field. While there has been a great deal of experimental research on Co|Ni multilayers, study of the ferromagnetic resonance linewidth and the magnetization damping of multilayers has yet to be reported.

In this paper, we present a study of the magnetic properties and the magnetization dynamics of sputtered [t Co|2t Ni]×N multilayers. We discuss the sample fabrication, the structural characterization of the films, and the experimental setup. Then the thickness dependence of the effective anisotropy field and the Landée g-factor is presented and analyzed. Finally, the magnetic damping parameter α is estimated and its thickness dependence is discussed.

2 Sample fabrication and experimental set-up

Two series of films with the layered structure ||Pt|Cu|[t Co|2t Ni]×N|Cu|Pt|| were fabricated, where N is the number of bilayer repeats. The Co|Ni layer thickness ratio was kept constant at 1 to 2, and t was varied between 0.1 and 0.6 nm. The Pt and Cu layers are 5 nm and 10 nm thick respectively. For one series of multilayers, the number of Co|Ni bilayer repeats was kept constant at N= 12 with $0.1 \leq t \leq 0.6$ nm. Thus, the total thickness d of the magnetic multilayer varied from 7.2 to 21.6 nm. For the other set of samples, N was chosen so that d is constant at 3.6 nm

Send offprint requests to:
Correspondence to: andy.kent@nyu.edu

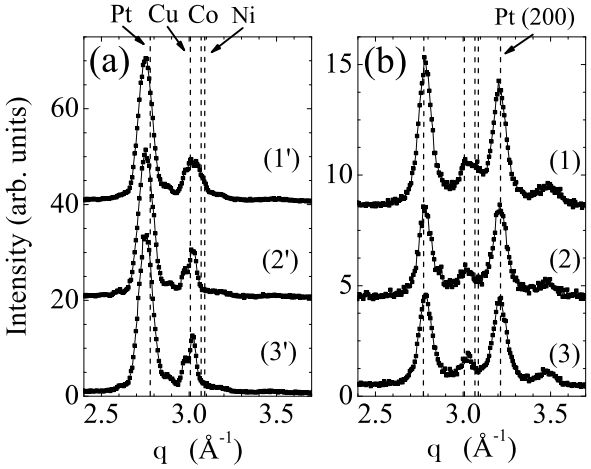

Fig. 1. The diffraction pattern (a) at 0° (along the [111] direction) and (b) at 54.74° (along the [200] direction) for [0.1 Co|0.2 Ni]×12 (1, 1'), [0.3 Co|0.6 Ni]×4 (2, 2') and [0.3 Co|0.6 Ni]×12 (3, 3'). The curves are shifted up for clarity. The dashed lines show the q value for bulk fcc (111) Pt (q=2.7735 $Å^{-1}$), Cu (q=3.0107 $Å^{-1}$), Co (q=3.07077 $Å^{-1}$) and Ni (q=3.0882 $Å^{-1}$).

with N= $1.2/t$. Note that $d = 3.6$ nm is in the range of the free layer thicknesses used in spin-transfer devices. The multilayers were prepared by DC magnetron sputtering at room temperature on oxidized Si wafers, with no applied magnetic field. The base pressure in the UHV system was 2×10^{-7} Torr and the Ar pressure was 1.7×10^{-3} Torr. The stacking of the individual Co and Ni layers was achieved by opening and closing shutters.

2.1 Structural characterization

Non-resonant x-ray diffraction (XRD) was carried out on films with magnetic layer structures of [0.1 Co|0.2 Ni]×12, [0.3 Co|0.6 Ni]×4, and [0.3 Co|0.6 Ni]×12 at 1.6295 Å (7.6084 keV) at NSLS beamline X16B (Figure 1). The wavelength was calibrated using an Al_2O_3 powder sample, and the intensity was collected with a solid state Bicron detector. In all films the Pt and Cu layers have a face centered cubic (fcc) structure evident from the (111) and (200) reflections present for both elements. In Figure 1a, the measurements were taken with the scattering vector along the sample normal, and here the (111) reflection dominates. In Figure 1b the sample was rotated by 54.74° about the incident beam so that the scattering vector probed along the [200] crystal orientation as defined for the [111] orientation aligned with the sample normal. Although both the (111) and (200) reflections can be seen in this geometry, there is an obvious enhancement of the (200) reflection (second set of peaks at higher q). These results are consistent with a textured film whose (111) orientation aligns along the sample normal. An unexpected finding is that while the (111) and (200) Pt

peaks are close to their nominal values at a sampling angle of 54.74° to the sample normal, the (111) peak shifts to lower q (expanded lattice) when measured along the sample perpendicular. This feature is present in all the films and indicates an expanded lattice. It is not expected that the strain could be induced from the Cu with a smaller lattice spacing, but the effect of in-plane strain and of the substrate with which the Pt is also in contact with could also play a role.

In order to quantitatively separate the Co and Ni from the Cu and to determine whether they also have a fcc structure we obtained resonant diffraction data from NSLS beamline X6B at both the Co and Cu K-edges, which minimizes Co and Cu elastic scattering contributions, respectively. For these measurements we studied the thickest sample [0.3 Co|0.6 Ni]×12 exclusively and focused on the out-of-plane (111) peak region where the scattering was strongest. Figure 2 shows that there appears to be four distinct peaks in this region. Two of these correspond well to nominal Cu (111) at 3.01 Å^{-1} and to a mix of nominal Co and Ni (111) (which are nearly lattice matched and are assumed to have similar structure and texture) at 3.07 Å^{-1} to 3.09 Å^{-1}. The peak between them can be explained by a Cu|Co+Ni intermediate region centered at 3.040 ± 0.005 Å^{-1} which forms a peak distinct from the bulk Cu and bulk Co+Ni. The fact that it is most prominent away from both the Cu and Co absorption edges indicates it contains the scattering from both elements. Finally, the lowest q peak at 2.98 Å^{-1} clearly decreases at the Cu K-edge (i.e. it involves Cu), does not change relative intensity when the photon energy is tuned to the Pt L3 edge (i.e. does not include Pt), and is unaffected by the total thickness of the Co and Ni layers. Thus, it is likely the result of strain on Cu by the Pt that has a slightly larger fcc lattice structure than bulk fcc Cu. The question remains open as to whether the intermediate Cu|Co|Ni peak is indeed a single lattice-matched region, or comprised of yet more overlapping sub-peaks of slightly different lattice spacing. With the present data we cannot say with certainty which case is true. However, the fact that the center of this intermediate peak does not shift in reciprocal space when going from the Co to the Cu K-edge is an indication that both the Co and the Cu could be fully lattice matched here. A new, more analytical method based on resonance scattering has been developed to analyze just such situation, and will be reported in a forthcoming article.

2.2 Experimental technique

FMR measurements were conducted at room temperature employing a coplanar waveguide (CPW) as an ac magnetic field generator and inductive sensor [9]. The CPW is made of a 200 nm thick Au film, deposited on a semi-insulating and polished 350 μm thick GaAs wafer. The metallic layer was patterned using a bi-layer photolithographic process. The microwave device was designed to have a characteristic impedance of 50 Ω above 4 GHz: the signal line is 50 μm

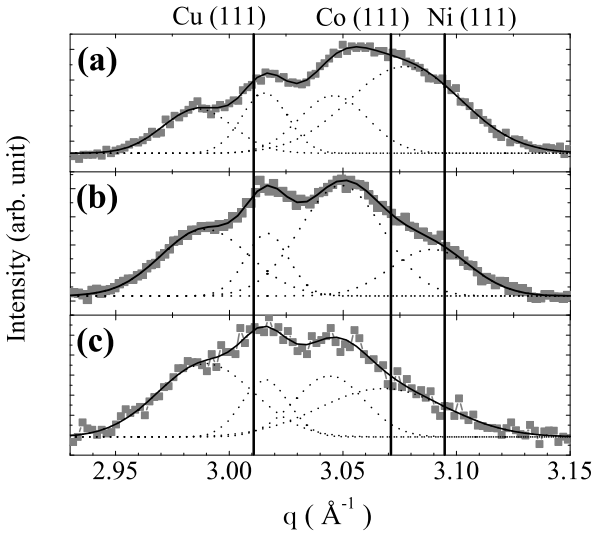

Fig. 2. The diffraction pattern of [0.3 Co|0.6 Ni]×12 (a) at the Cu K-edge (8.979 keV), (b) off resonance (9.5 keV) and (c) at the Co K-edge (7.709 keV). The solid black lines are the resulting Gaussian multi-peaks fit.

wide and is separated of the ground plate by a gap of 32 μm. The CPW was placed into a brass cavity and connected directly to the ports of a Network Analyzer. Care was taken to avoid magnetic components in the cavity and in all contacts to the CPW. FMR spectra were measured by placing the magnetic sample metal face down on the CPW. For a fixed frequency (4 to 50 GHz), the external magnetic field was swept while measuring the S-parameters of the transmission line. The measurements were conducted with dc fields up to 10 kG. Figure 3a shows the geometry of the measurements. The applied field was monitored with a Hall probe sensor, and the calibration of the sensor was verified using electron paramagnetic resonance (EPR) on 2,2-diphenyl-1-picrylhydrazyl (dpph), a spin 1/2 system. The cavity was mounted on a rotating arm that enables FMR measurements in the parallel geometry ($\boldsymbol{H}$ in the film plane), in the perpendicular geometry ($\boldsymbol{H}$ normal to the film plane), and as a function of the angle of the dc field and the film plane. All measurements were performed with the applied field perpendicular to the ac magnetic field.

The FMR response of a 50 nm Co and of a 50 nm Ni film sputtered on Si-SiO_2 substrates was measured (Figure 4). The magnetic layers have the same layer environment as the Co|Ni multilayers, with a ||5 nm Pt|10 nm Cu| base layer and a |10 nm Cu|5 nm Pt|| top layer. The frequency dependence of the resonance field in the parallel geometry is fitted to the Kittel formula [10]. For the 50 nm Co film, the estimated value of the magnetization density $M_{\rm s}^{\rm Co} = 1408 \pm 16$ emu/cm^3 and the measured g-factor $g^{\rm Co} = 2.148 \pm 0.009$ agrees within 0.5% with the parameters of the bulk material, $M_{\rm s}$=1400 emu/cm^3 and $g = 2.145$. For the film with 50 nm Ni, the experimental g-factor value $g^{\rm Ni} = 2.208 \pm 0.018$ is

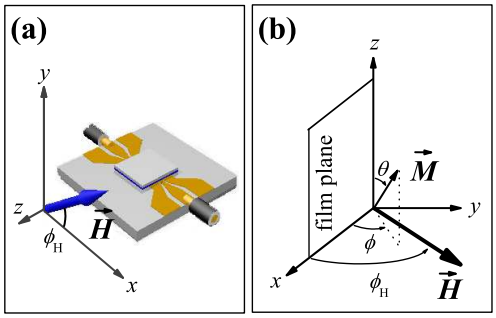

Fig. 3. a) Geometry of the FMR measurements. The Network Analyzer ports are connected directly to the CPW. b) Direction of the applied magnetic field $\boldsymbol{H}$ and the magnetization $\boldsymbol{M}$. Measurements were conducted with the field in the (x-y) plane, i.e $\theta = \pi/2$.

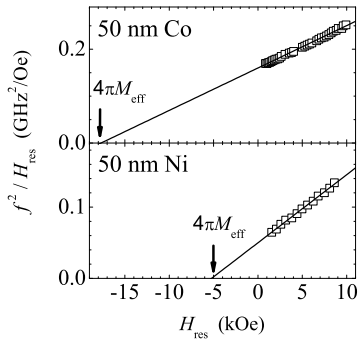

Fig. 4. Frequency dependence of the resonance field $H_{\rm res}$ of ||Pt|Cu|50 nm Co|Cu|Pt|| and ||Pt|Cu|50 nm Ni|Cu|Pt|| sputtered on Si-SiO_2 substrate. The frequency dependence of $H_{\rm res}$ is fitted to $f^2/H_{\rm res} = (g\mu_B/\hbar)(H_{\rm res} + 4\pi M_{\rm eff})$ where the zero frequency intercept gives $4\pi M_{\rm eff}$ and the slope provides the g-factor.

in good agreement with the literature value ($g = 2.21$), whereas the estimated magnetization density $M_{\rm s}^{\rm Ni} = 416 \pm 14$ emu/cm^3 is about 15% smaller than that of bulk Ni. Because fcc Co and Ni have about same lattice constant, $a_{\rm Co} = 3.545$ Å [11] and $a_{\rm Ni} = 3.524$ Å [12] respectively and same density (≈8.91 g/cm^3), the magnetization density of [t Co|2t Ni]×N is determined from the average $M_{\rm s} = (M_{\rm s}^{\rm Co} + 2M_{\rm s}^{\rm Ni})/3$, hence $M_{\rm s} = 747$ emu/cm^3. Note that the magnetic materials are immiscible at room temperature [13]. We assume that the magnetization density of the individual Co and Ni layers is thickness independent.

3 Theory

The geometry of the vectors is shown in Figure 3b. $\boldsymbol{M}$ is the magnetization, $\boldsymbol{H}$ is the applied magnetic field, and θ, ϕ and $\phi_{\rm H}$, are the angles associated with these vectors. The film is in the (x-z) plane. We assume that the Co and Ni layers are strongly ferromagnetically exchange coupled, and as a consequence the magnetization of the multilayer can be approximated as a macrospin. The applied field is chosen to remain in the (x-y) plane. For a polycrystalline film all directions in the film plane are equivalent, so $\boldsymbol{M}$ will also remain in the (x-y) plane, hence $\theta = \pi/2$. The total magnetic energy density of the system E_t is given by the expression [14]:

$$E_t = -M_{\rm s}H(\cos\phi\cos\phi_{\rm H} + \sin\phi\sin\phi_{\rm H}) + 2\pi M_{\rm s}^2\sin^2\phi - (K_1 + 2K_2)\sin^2\phi + K_2\sin^4\phi. \quad (1)$$

The first and second term represent the Zeeman energy and the magnetostatic energy respectively. The last two terms are the uniaxial anisotropy energy, where K_1 and K_2 are the first and second order effective uniaxial anisotropies. K_1 and K_2 include the surface anisotropy (Néel-type) energy and the magneto-elastic anisotropy energy. The surface anisotropy originates from the broken symmetry at interfaces of the multilayer [15] and the strain can be induced by the lattice mismatch between the layers. With our notation, positive values of the anisotropy constants favor magnetization normal to the film plane. For a given direction of the applied magnetic field, the equilibrium position of the magnetization is calculated from $(\partial E_t/\partial\phi) = 0$ and is given by the relation:

$$2H_{\rm res}\sin(\phi_{\rm H} - \phi) = 4\pi M_{\rm eff}\sin 2\phi, \quad (2)$$

where the effective demagnetization field is defined as:

$$4\pi M_{\rm eff} = 4\pi M_{\rm s} - \frac{2K_1}{M_{\rm s}} - \frac{4K_2}{M_{\rm s}}\cos^2\phi. \quad (3)$$

If K_2 is not negligible, then $4\pi M_{\rm eff}$ is dependent on angle and for K_1 and K_2 positive $(4\pi M_{\rm eff})^{\perp}$ is larger than $(4\pi M_{\rm eff})^{||}$.

3.1 Resonance field

From the Smit and Beljers formula [16], the resonance condition is:

$$\omega = \gamma\sqrt{H_1 H_2}, \quad (4)$$

where:

$$H_1 = H\cos(\phi_{\rm H} - \phi) - 4\pi M_{\rm eff}\sin^2\phi, \quad (5)$$

and

$$H_2 = H\cos(\phi_{\rm H} - \phi) + 4\pi M_{\rm eff}\cos 2\phi + \frac{2K_2}{M_{\rm s}}\sin^2 2\phi. \tag{6}$$

$\gamma(= g\mu_B/\hbar)$ is the gyromagnetic ratio. For the the parallel geometry ($\phi_{\rm H} = 0^{\rm o}$) and perpendicular geometry ($\phi_{\rm H} = 90^{\rm o}$), the resonance conditions are:

$$\left(\frac{\omega}{\gamma}\right)^2_{||} = H_{\rm res}\left(H_{\rm res} + 4\pi M_{\rm s} - \frac{2K_1}{M_{\rm s}} - \frac{4K_2}{M_{\rm s}}\right), \tag{7}$$

and

$$\left(\frac{\omega}{\gamma}\right)_{\perp} = H_{\rm res} - 4\pi M_{\rm s} + \frac{2K_1}{M_{\rm s}}. \tag{8}$$

3.2 Linewidth and damping

It is common to express the frequency dependence of the full width at half maximum in the following form [10]:

$$\triangle H(f) = \triangle H_0 + \frac{4\pi\alpha}{\gamma} f. \tag{9}$$

$\triangle H_0$ describes an inhomogeneous broadening due to sample imperfections and is assumed to be independent of the frequency. The second term, known as the intrinsic linewidth, is proportional to the magnetic damping parameter α and scales linearly with the frequency f. By measuring the FMR signal at several frequencies, α can be extracted from the slope of the curve $\triangle H(f)$. The intercept with the zero frequency axis gives $\triangle H_0$.

4 Experimental data and discussion

4.1 Resonance field

Figure 5 presents typical normalized FMR peaks of a [0.2 Co|0.4 Ni]×12 multilayer for different field directions. The presence of a single resonance for all the three measurements geometries suggests that the multilayer behaves as a single magnetic film and that the macrospin picture is appropriate to describe the FMR response. The absorption lines were normalized by substracting the background signal and dividing by the relative change in transmission at resonance. The lineshape of the FMR curves is typically Lorentzian. We also observed asymmetric lineshapes at some frequencies, which we attribute to the mixing of the absorptive and dispersive components of the susceptibility [17], due to "poor" deembedding of the transmission line.

The frequency dependence of $H_{\rm res}$ versus frequency for in-plane and normal to the plane field directions, and the angular dependence of the resonance field are shown in Figure 6. The effective demagnetization in the parallel geometry

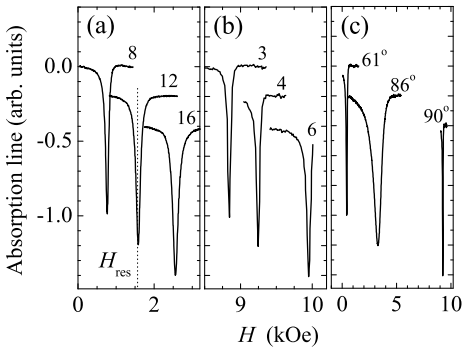

Fig. 5. Typical absorption lines of [0.6 Co|1.2 Ni]×12 (a) at 8, 12 and 16 GHz with the applied field $\boldsymbol{H}$ in the film plane (b) at 3, 4 and 6 GHz with $\boldsymbol{H}$ normal to the plane and (c) at 4 GHz for a selection of out-of-plane angles ($\phi_{\rm H}$ =61°, 86° and 90°).

$(4\pi M_{\rm eff})^{||} = 4801 \pm 36$ G and the g-factor $g = 2.221 \pm 0.006$ are determined using Eq. 7 and the method described in section 2.2. Eq. 8 is used to fit $H_{\rm res}$ versus f in the perpendicular geometry with $(4\pi M_{\rm eff})^{\perp}$ as the only fitting parameter, and with the assumption that the g-factor is isotropic. $(4\pi M_{\rm eff})^{\perp} = 5230 \pm 8$ G is about 9% larger than $(4\pi M_{\rm eff})^{||}$. This provides evidence for a non-negligible second order anisotropy term. Using Eq. 7 and 8, the effective uniaxial anisotropy constants $K_1 = 1.551 \times 10^6$ erg/cm^3 and $K_2 = 0.080 \times 10^6$ erg/cm^3 are calculated. The extracted parameters are used to fit the angular dependence of $H_{\rm res}$. As shown in Figure 6, the fit (solid line) and the experimental data $H_{\rm res}$ versus $\phi_{\rm H}$ at $f = 4$ GHz agree very well. In fact, we also found very good agreement with measurements conducted at 8 and 12 GHz. When comparing the fit and the experimental data, chi-square increases by a factor 2 when K_2 is set to zero. K_1 and K_2 are positive and $K_1 >> K_2$ which means that they favor the magnetization out of the film plane. Nevertheless, it is clear from the shape of the curve $H_{\rm res}(\phi_{\rm H})$, where $(H_{\rm res})^{\perp} > (H_{\rm res})^{||}$, that the preferential direction for the magnetization of the multilayer is in the film plane.

For frequencies above 25 GHz, an additional resonance peak is observed in the absorption line of the thickest magnetic multilayer [0.6 Co|1.2 Ni]×12 (inset of Figure 7). The frequency dependence of this resonance peak suggests that it is associated with a spin-wave resonance mode. The high-order resonance field $H_{\rm res}^{(1)}$ and its amplitude are smaller than that of the uniform resonance mode. In a model proposed by Kittel [18], the field splitting with respect to the uniform mode is described by $H_n = 2Ak^2/M_{\rm s}$, where A is the exchange constant. If there is no pinning of the surface spins at the bottom and top interfaces then $k = (n-1)\pi/d$, where n is the perpendicular standing spin wave number and d is the total thickness of the magnetic film. Using a weighted value for the exchange constant of the Co|Ni multilayer $A = (A^{\rm Co} + 2A^{\rm Ni})/3$ with $A^{\rm Co} = 1.3 \times 10^{-6}$ erg/cm [19] and $A^{\rm Ni} = 0.75 \times 10^{-6}$ erg/cm [20], we find $n = 1.96 \pm 0.03 \approx 2$, which corresponds to the surface spin wave of the 1$^{\rm st}$ order. The Kittel model assumes

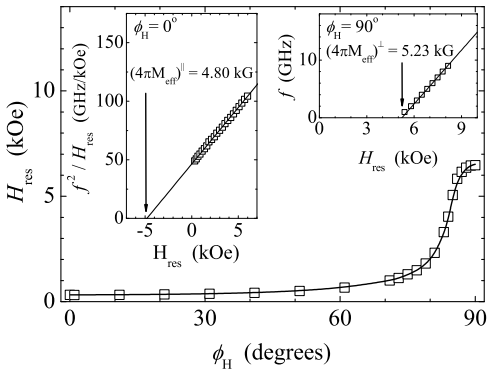

Fig. 6. The angular dependence of $H_{\rm res}$ of [0.3 Co|0.6 Ni]×12 multilayer at 4 GHz, where $\phi_{\rm H} = 0^{\rm o}$ corresponds to the parallel geometry. The insets show the frequency dependence of the resonance field for $\phi_{\rm H} = 0^{\rm o}$ and $\phi_{\rm H} = 90^{\rm o}$, and the corresponding effective demagnetization field $(4\pi M_{\rm eff})^{||}$ and $(4\pi M_{\rm eff})^{\perp}$.

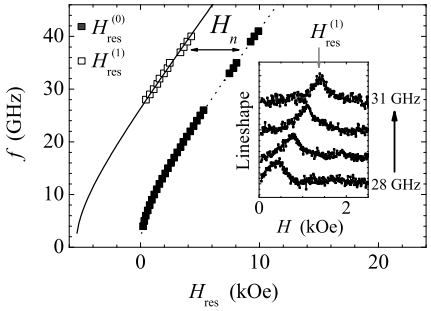

Fig. 7. The frequency dependence of the resonance field of the uniform mode $H_{\rm res}^{(0)}$ (filled symbols) and of the spin wave mode $H_{\rm res}^{(1)}$ (open symbols) of the multilayer [0.6 nm Co|1.2 nm Ni]×12 in the parallel geometry. The peak separation is $H_n \simeq 5.4$ kOe. The insert shows the absorption line of the high frequency resonance peak at f =28, 29, 30 and 31 GHz.

that the magnetization density is uniform across the film thickness. Such a spin wave mode is therefore not expected to be observed with a uniform ac field since $\sum \boldsymbol{m_z} = 0$. Using approximations for the conductivity of the magnetic multilayer and its permeability at high field (off resonance), the ac field attenuation through the multilayer [0.6 nm Co|1.2 nm Ni]×12 is estimated to be about 3% at 30 GHz. We suspect that inhomogeneity of the ac field and the structural asymmetry of our Co|Ni multilayer film, with two different outer interfaces, Cu|Co and Ni|Cu, can lead to $\sum m_z \neq 0$, and excitation of spin-wave modes.

The thickness dependence of the effective anisotropy constants of the multilayers [t Co|2t Ni] with 12 repeats and with $1.2/t$ repeats is shown in Figure 8. In the thickness range $0.1 \leq t \leq 0.6$ nm, K_1 is positive and greater than K_2, and it exhibits a maximum value of about $1.8{\times}10^6$ erg/cm^3. K_1 of the multilayers with 12 repeats increases by

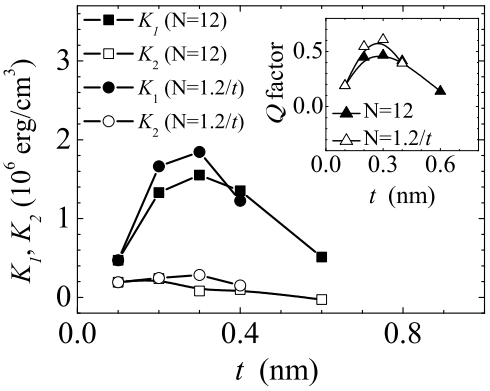

Fig. 8. Thickness dependence of the anisotropy constants K_1 and K_2 and of the quality factor Q. The solid lines are guides-to-the-eye.

a factor 3 when t decreases from 0.6 nm to 0.3 nm. The second order anisotropy term is negative for $t = 0.6$ nm ($K_2 = -0.028 \times 10^6$ erg/cm^3) and changes to positive values for smaller t. For $0.1 \leq t \leq 0.4$ nm, K_1 and K_2 of multilayers of 12 and $1.2/t$ Co|Ni repeats have very similar t dependence.

In Figure 9 the g-factor as a function of the thickness t is presented. The Landé g-factor of the films with same magnetic layer thickness (3.6 nm) varies with t in the same way as that of the multilayers with constant number of repeats. This suggests that g does not depend on the total thickness of the multilayer, and it is the thickness of the Co and Ni layers that induces the change in g. The dashed line in Figure 9 shows the calculated value of the g-factor of the multilayers based on a geometric average [21]:

$$g_{\text{eff}} = \frac{M_{\text{s}}^{\text{Co}} + 2M_{\text{s}}^{\text{Ni}}}{M_{\text{s}}^{\text{Co}}/g^{\text{Co}} + 2M_{\text{s}}^{\text{Ni}}/g^{\text{Ni}}}. \tag{10}$$

Using the values found for the 50 nm Co and 50 nm Ni films, we find $g_{\text{eff}} = 2.170 \pm 0.058$. The inset Figure 9 shows g versus $1/t$. The data points fall on a line for $t \geq 0.2$ nm. The intercept of the linear fit with the t^{-1}=0 axis gives $g = 2.170 \pm 0.012$ which agrees with the value of g_{eff}. A similar linear fit for the film with N=$(1.2/t)$ gives $g = 2.163 \pm 0.024$.

4.2 Discussion of resonance field

In the study of magnetic films with large PMA, the dimensionless quality factor Q is often used as a figure of merit. Q is defined by the ratio of the uniaxial anisotropy to the demagnetizing energy. In the limit that the PMA field overcomes the demagnetization field, the normal to the film plane becomes the axis of easy magnetization and $Q > 1$.

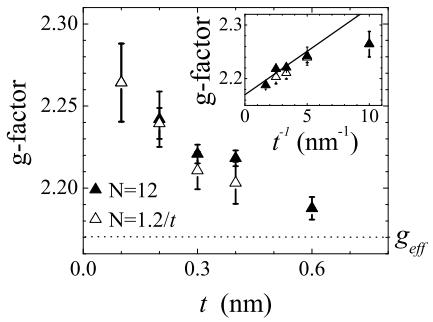

Fig. 9. Thickness dependence of the g factor for Co|Ni multilayers of 12 bilayer repeats (filled symbols), and multilayers with constant layer thickness (open symbols). The inset shows g as a function of $1/t$. The solid line is the best fit of $g(1/t)$ for films with N=12 and without taking into account the data point at $1/t = 10$ nm^{-1}.

The inset of Figure 8 shows the dependence of $Q = (K_1 + K_2)/2\pi M_s^2$ as a function of t. The quality factor of the Co|Ni sputtered multilayers does not exceed 0.7. The magnetization of the films remains preferentially in the film plane, in contrast to what has been observed for evaporated multilayers of the same Co:Ni thickness ratio [22]. The result can be in parts explained by the crystallographic growth direction of the underlayer that does not promote a highly textured (111) film. The diffraction pattern of the multilayers exhibit a (111) Pt peak, but also a peak that corresponds to Pt (200). Zhang *et al*. conducted XRD and magnetometry measurements on sputtered Co|Ni grown on Au and Ag base layer [23]. The authors found that only the multilayers grown on Au have the magnetization easy axis normal to the film plane. The XRD study showed that the Ag (111) intensity peak is 10 times smaller than that of Au (111), with the presence of a second peak of intensity corresponding to Ag (200).

The magneto-elastic contribution arises from the strain induced by the lattice mismatch η between adjacent layers. The largest strain originates from the lattice mismatch at the Cu|Co interface where $|\eta_{\mathrm{Cu|Co}}| \approx 1.8\%$, compared to $|\eta_{\mathrm{Co|Ni}}| \approx 0.6\%$ at the Co|Ni interface. The anisotropy constants of the films with same multilayer thickness depends strongly on t. Therefore, the interfaces Cu|Co and Ni|Cu do not appear to play a significant role in the t dependence of the anisotropy constants. Consequently, the variation of the anisotropies with t is associated with the Co|Ni interfaces, as predicted by Daalderop *et al.* [8]. From *ab-initio* calculations, the authors found that in the multilayers, the interface anisotropy is controlled by d-state occupancy near the Fermi level at the Co|Ni interface. The presence of an optimum thickness t for large K_1 value can be understood as follows. With increasing t, the number of Co|Ni interfaces per unit volume decreases and K_1 decreases. In the limit of very small t, the magnetic layers are not uniform. The multilayer breaks down into an alloy-type structure and K_1 decreases.

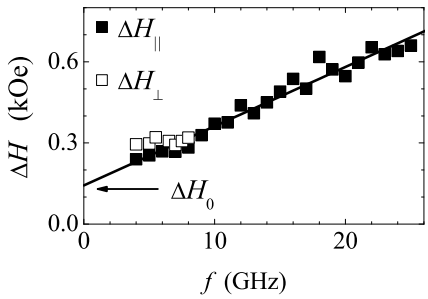

Fig. 10. Frequency dependence of the linewidth in the parallel ($\triangle H_{||}$) and perpendicular ($\triangle H_{\perp}$) geometry of the film [0.2 nm Co|0.4 nm Ni]×6. The extrinsic contribution $\triangle H_0$ and the intrinsic contribution $\triangle H/df$ to the linewidth are extracted from the linear best fit of $\triangle H_{||}(f)$ (solid line).

The g-factor is related to the ratio of the orbital to spin moments μ_ℓ/μ_s by $\mu_\ell/\mu_s = (g-2)/2$ [24], hence one deduces that μ_ℓ/μ_s increases by 3.4% when t is decreased from 0.6 nm to 0.1 nm. This enhancement depends on the thickness of the individual Co and Ni layers. Significant increase of the ratio μ_ℓ/μ_s, up to 40% have been reported for ultrathin FM in contact with a NM [25]. The enhancement was attributed to the breaking of the symmetry at the interface, where the orbital moment of the surface/interface atoms is enhanced compared to that of the bulk atoms.

4.3 Linewidth and magnetic damping

The linewidth was studied as a function of frequency in the parallel and the perpendicular geometry. Figure 10 shows typical data for [0.2 nm Co|0.4 nm Ni]×12 multilayer. The linewidth in the parallel geometry $\triangle H_{||}$ and in perpendicular geometry $\triangle H_{\perp}$ follows similar frequency dependence, and increases with frequency. $\triangle H_{\perp}$ is slightly larger than $\triangle H_{||}$ at low frequencies (4-6 GHz), which we attribute to a small misalignment of the applied field with the normal to the film plane. Exchange narrowing can also lead to $\triangle H_{\perp} > \triangle H_{||}$ [26]. $\triangle H$ in the parallel geometry depends linearly on frequency, with a zero frequency offset. The inhomogeneous broadening $\triangle H_0 = 143 \pm 16$ Oe and the damping parameter $\alpha = 0.0343 \pm 0.0017$ are extracted from the best linear fit (Eq. 9). Note that the inhomogeneous ac field due to the finite width of the transmission line can lead to the broadening of the linewidth [27]. The additional linewidth increases with the magnetic film thickness and is inversely proportional to the frequency. For the thickest magnetic multilayer ($d = 21.6$ nm), we estimate the additional linewidth at 5 GHz to be less than 1% of the measured linewidth. Spin wave contributions to the linewidth from the CPW geometry can therefore be neglected. The dependence of $\triangle H_{||}$ versus frequency is linear for most samples. Only the thinnest film [0.1 nm Co|0.2 nm Ni]×12 exhibits a non linear dependence on frequency so that α and $\triangle H_0$ could not be determined (Figure 11). A linear fit of $\triangle H_{||}$ as a

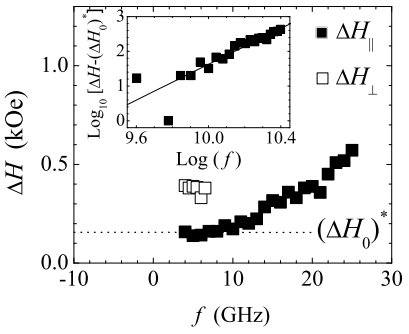

Fig. 11. The linewidh versus frequency for the film [0.1 Co|0.2 Ni]×12 in the parallel geometry. $(\triangle H_0)^*$ is the extrapolated linewidth when f approaches zero frequency linewidth. The inset shows the data in $\mathrm{Log_{10}}$-$\mathrm{Log_{10}}$ scale, and the linear best fit (solid line).

function of frequency in a $\mathrm{Log_{10}}$-$\mathrm{Log_{10}}$ plot scale gives $n = 2.58 \pm 0.30$ with $\triangle H_{||} \propto f^n$. The behaviour might originate from two-magnon scattering contribution to the linewidth induced by the film roughness. Indeed, Twisselmann *et al.* found that a 64 nm Py film grown on a highly oriented roughness shows a non linear in-plane linewidth frequency dependence, when the dc field is applied perpendicular to the scratches [28]. The magnetic damping parameter and the extracted inhomogeneous contribution $\triangle H_0$ to the linewidth of the multilayers is shown in Figure 12. α and $\triangle H_0$ of the films with N=12 increases monotonically with decreasing t. The thickness dependence t of $\triangle H_0$ of the films with $N = 1.2/t$ is not clear. The inset of Figure 12a shows $\triangle H_0$ as a function of $1/d^2$, where d is the total thickness of the magnetic multilayer. The extrinsic contribution to the linewidth increases linearly with d^{-2}. The damping of the films with $t = 0.2$ and 0.3 nm and thickness 3.6 nm is 40% larger than that of the film with $t = 0.4$ nm. The largest damping values are found for the films 3.6 nm thick, which are the thinnest magnetic multilayers.

4.4 Discussion of Enhanced Damping

The enhancement of the magnetic damping constant in thin magnetic films can originate from several mechanisms. It is generally believed that the spin-orbit interaction in a ferromagnet, which couples the spin to the lattice, plays a dominant role in the damping mechanism. The following expression was theoretically derived [29]:

$$\mathrm{G} \propto \triangle g^2, \tag{11}$$

where $\triangle g$ is the deviation of the Landé g-factor from the free electron value 2.0023 and G is the Gilbert damping constant defined by G= $\alpha \gamma M_\mathrm{s}$. Figure 13 shows the Gilbert damping constant versus $(\triangle g)^2$ for the two series of multilayers. For a given Landé g-factor value, the damping is largest for the film 3.6 nm thick.

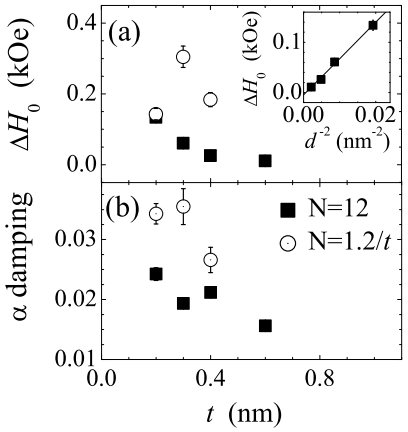

Fig. 12. Dependence of the extrinsic contributions $\triangle H_0$ and the damping α extracted from the slope $d\triangle H/df$ for multilayers with same number of bilayer repeats (N=12) and for films with same thickness (N=1.2/t). The inset in (a) shows $\triangle H_0$ versus $1/d^2$ for the multilayers with N=12, where d is the total multilayer thickness. The solid line is the linear best fit of $\triangle H_0$ versus $1/d^2$.

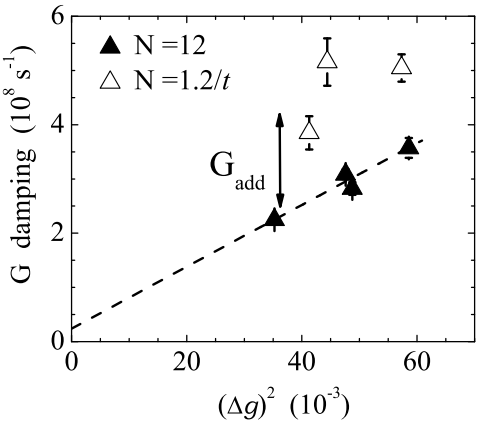

Fig. 13. The Gilbert damping constant G as a function of $(\triangle g)^2 = (g - 2.0023)^2$. G_{add} is the additional damping from spin pumping: the difference between the damping of the thickest film ([0.6 nm Co|1.2 nm Ni]×12) and that of the films of 3.6 nm thickness. The dashed line is a guide to the eye.

A mechanism that can explain the enhanced Gilbert damping in the 3.6 nm thick multilayer films is the spin-pumping [30]. The precessing magnetization of the Co|Ni multilayers generates a spin current that flows through the adjacent Cu layers and relaxes in Pt, a strong spin scatterer. As a consequence, the damping is enhanced. For a

symmetric structure where the FM is embedded between ||NM2|NM1| bilayers, the enhanced damping $\alpha_{\rm eff}$ is:

$$\alpha_{\rm eff} = \alpha_0 + \frac{g\mu_B}{2\pi M_{\rm s}} \frac{\tilde{g}_{\rm eff}^{\uparrow\downarrow} S^{-1}}{d}. \tag{12}$$

α_0 is the residual damping (bulk) and the second term represents the additional damping from spin pumping where $\tilde{g}_{\rm eff}^{\uparrow\downarrow} S^{-1}$ is the effective spin mixing conductance. Eq. 12 is valid when the NM2 is a perfect spin sink and the thickness of the NM1 is much smaller than the spin diffusion length of the material. Pt is known to act as a perfect spin sink and the Cu layer of 10 nm is much thinner than the spin diffusion length at room temperature $\lambda_{\rm sf} = 350$ nm [31]. The additional damping induced by spin pumping effect in the 3.6 nm film is the difference between G of the thickest multilayer film (21.6 nm) and that of the 3.6 nm films (Figure 13). Using an average value for the g-factor, we obtain $\alpha_{\rm add} \approx 0.015$. The effective spin mixing conductance of sputtered Co layer embedded between ||Pt|Cu| bilayer was found to be $g_{\rm eff}^{\uparrow\downarrow} S^{-1} = (1.63 \pm 0.18) \times 10^{15}$ cm^{-2} [32]. The additional damping computed using Eq. 12 is $\alpha_{\rm add} \approx 0.020$. This is in the range of the value found using the experimental data.

5 Conclusion

This FMR study on several sputtered t Co|2t Ni multilayers shows in-plane preferential orientations, and also perpendicular effective anisotropy K_1 as large as 2.8×10^6 erg/cm^3. We have provided evidence that to understand the frequency dependence and angular dependence of the resonance field, second order anisotropy terms have to be considered. The Landé factor increases with decreasing t and the enhancement depends on the thickness of the individual Co and Ni layers. The thickness dependence of g is explained in terms of the lowering of the symmetry at the Co|Ni interface. The extrinsic and the intrinsic contribution to the FMR linewidth increases with decreasing thickness t of the individual layers. $\triangle H_0$ follows a $1/d^2$ dependence. The enhancement of the magnetic damping is attributed to the increase of spin-orbit interaction and to the spin-pumping. In order to clarify this point it would be interesting to study similar magnetic multilayers without the Pt layers. Indeed, without adjacent layers with strong spin-orbit scattering, the additional damping is expected to be weak.

The possibility to tune the easy plane anisotropy by changing the thickness of the individual magnetic layers makes the Co|Ni multilayer an interesting magnetic structure to be integrated in spin-transfer devices. In addition, the damping while larger than that of Permalloy is similar to that of Co ultrathin films. It would also be interesting to compare the high frequency dynamics of films grown with different underlayers and deposition methods.

We thank Dr. G. de Loubens for fruitful discussions. This research is supported by NSF-DMR-0405620. Use of the National Synchrotron Light Source, Brookhaven National Laboratory, was supported by the U.S. Department of Energy, Office of Science, Office of Basic Energy Sciences, under Contract No. DE-AC02-98CH10886.

References

1. see, for example, J. A. Katine, F. J. Albert, and R. A. Buhrman, E. B. Myers, and D. C. Ralph, Phys. Rev. Lett. **84**, 3149 (2000) ; B. Öezyilmaz, A. D. Kent, D. Monsma, J. Z. Sun, M. J.Rooks, and R. H. Koch, Phys. Rev. Lett. **91**, 067203 (2003).
2. Y. Tserkovnyak, A. Brataas, G. E. W. Bauer, Phys. Rev. B **66**, 224403 (2002).
3. B. Heinrich, Y. Tserkovnyak, G. Woltersdorf, A. Brataas, R. Urban, and G. E. W. Bauer, Phys. Rev. Lett. **90**, 187601 (2003) ; J. Z. Sun, B. Öezyilmaz, W. Y. Chen, M. Tsoi, and A. D. Kent, J. Appl. Phys. **97**, 10C714 (2005).
4. J-M. L. Beaujour, J. H. Lee, A. D. Kent, K. Krycka and C-C. Kao, Phys. Rev. B **74**, 214405 (2006).
5. J. Z. Sun, Phys. Rev. B **62**, 570 (2000).
6. A. D. Kent, B. Öezyilmaz, and E. del Barco, Appl. Phys. Lett. **84**, 3897 (2004).
7. S. Mangin, D. Ravelosona, J. A. Katine, M. J. Carey, B. D. Terris, E. E. Fullerton, Nature Materials **5** (3), 210 (2006).
8. G. H. O. Daalderop, P. J. Kelly and F. J. A. de Broeder, Phys. Rev. Lett. **68**, 682 (1992).
9. W. Barry, I.E.E.E Trans. Micr. Theor. Techn. MTT **34**, 80 (1996).
10. see, for example, D. L. Mills and S. M. Rezende in Spin Dynamics in Confined Magnetic Structures II (Eds. B. Hillebrands and K. Ounadjela), pp. 27-58, (Springer, Heidelberg 2002).
11. E. A. Owen and D. Madoc Jones, Proc. Phys. Soc. B **67**, 456 (1954).
12. X. D. Liu, H. Y. Zhang, K. Lu and Z. Q. Hu, J. Phys.: Condens. Matter. **6**, L497 (1994).
13. C. W. Su, Y. D. Yao, C. S. Shern, J. Magn. Magn. Mater. **282**, 84 (2004).
14. C. Chappert, K. Le Dang, P. Beauvillain, H. Hurdequint, D. Renard, Phys. Rev. B **34** (5), 3192 (1986).
15. L. Néel, J. Phys. Radium **15**, 225 (1954).
16. S. V. Vonsovskii, Ferromagnetic Resonance (Pergamon, Oxford), (1966).
17. S. S. Klarickal, P. Krivosik, M. Wu, C. E. Patton, M. L. Schneider, P. Kabos, T. J. Silva, J. P. Nibarger, J. Appl. Phys. **99**, 093909 (2006).
18. C. Kittel, Phys. Rev. **110**, 1295 (1958).
19. P. E. Tannenwald, Phys. Rev. **121**, 715 (1961).
20. D.H. Martin, Magnetism in Solids (Iliffe books, London), (1967) p.67.
21. R. K. Wangsness, Phys. Rev. **91**, 1085 (1953).
22. P. J. H. Bloemen, W. J. M. de Jonge and F. J. A. den Broeder, J. Appl. Phys. **72**, 4840 (1992).

23. Y. B. Zhang, P. He, J. A. Woollam, J. X. Shen, R. D. Kirby and D. J. Sellmyer, J. Appl. Phys. **75**, 6495 (1994).

24. M. Farle, Rep. Prog. **61**, 755 (1998) and ref. therein.

25. M. Tischer, O. Hjortstam, D. Arvanitis, J. H. Dunn, F. May, K. Baberschke, J. Trygg, J. M. Wills, B. Johansson and O. Eriksson, Phys. Rev. Lett. **75** (8), 1602 (1995) ; A. Hahlin, J. H. Dunn, O. Karis, P. Poulopoulos, R. Nüthel, J. Lindner and D. Arvanitis, J. Phys.: Condens. Matter. **15**, S573 (2003).

26. H. Hurdequint, J. Magn. Magn. Mater. **242-245**, 521 (2002).

27. G. Counil, J-V. Kim, T. Devolder, C. Chappert, K. Shiegeto and Y. Otani, J. Appl. Phys. **95** (10), 5646 (2004).

28. D. J. Twisselmann and R. D. McMichael, J. Appl. Phys. **93**, 6902 (2003).

29. R. Elliott, Phys. Rev. **96**, 266 (1954).

30. Y. Tserkovnyak, A. Brataas, G. E. W. Bauer, B. I. Halperin, Rev. Mod. Phys. **77**, 1375 (2005).

31. F. J. Jedema, A. T. Filip, and B. J. van Wees, Nature (London) **410**, 345 (2001).

32. J.-M. L. Beaujour, W. Chen, A. D. Kent, and J. Z. Sun, J. Appl. Phys. **99**, 08N503 (2006).